Columnar Liquid Crystals from Star-Shaped Conjugated Mesogens as Nano-Reservoirs for Small Acceptors

Martin Lambov,[a] Nicola Hensiek,[a] Ann-Christin Pöppler,*[a] and Matthias Lehmann*[a, b]

Shape-persistent conjugated mesogens with oligothiophene arms of different lengths have been synthesized. Such mesogens possess free intrinsic space between their conjugated arms. They form columnar liquid-crystalline phases, in which the void is filled by dense helical packing in the neat phase similar to an oligo(phenylene vinylene) derivative of equal size. The void can also be compensated by the inclusion of the small acceptor molecule 2,4,7-trinitrofluorenone. In solution, the acceptor interacts with the core as the largest π-surface, while in the solid material, it is incorporated between the arms and sandwiched by the star-shaped neighbours along the columnar assemblies. The TNF acceptors are not nanosegregated from the star-shaped donors, thus the liquid crystal structure converts to a nano-reservoir for TNF (endo-receptor). These host–guest arrangements are confirmed by comprehensive X-ray scattering experiments and solid-state NMR spectroscopy. This results in ordered columnar hexagonal phases at high temperatures, which change to helical columnar mesophases or to columnar soft crystals at room temperature.

Introduction

In the last decades, donor-acceptor materials have been of enormous interest owing to their application in organic conducting[1] and semiconducting materials for photovoltaic applications.[2,3] Often, fullerene derivatives were the choice of acceptor molecules, but they are increasingly substituted by small molecular non-fullerene acceptors such as naphthalene bisimides, perylene bisimides, or donor-acceptor structures with strong acceptors bearing cyano groups.[4,5] One of the smallest strong acceptor molecules is 2,4,7-trinitrofluorenone (TNF), which has been utilised to stabilize columnar phases of discotic molecules.[6–17] They were proposed to form charge transfer (CT) complexes being sandwiched between two aromatic donor surfaces. This was evidenced by polarized UV-Vis spectroscopy showing the charge transfer complex in the direction of the columns[8] and the often most stable liquid crystal (LC) phases at the 1:1 stoichiometry.[14] In metallomesogens, TNF was proposed to be sandwiched acting as a space-filler and – through the CT interaction - preventing the molecular rotation in order to stabilise biaxial SmA phases.[18–20] However, some references highlight also other structures, in which donors and acceptors are separated in close proximity.[17,21,22] Such structures are known to be highly conductive as found for CT salts, which are organic crystals with strong donors and acceptors packed in the crystal side by side.[1,23] Therefore, triphenylene-TNF mixtures have been reinvestigated recently and the authors postulated TNF to be segregated in the tail structure, but no simultaneous donor and acceptor percolation paths could be observed.[24,25]

In our effort to study shape-persistent star mesogens and their function as hosts for either supramolecular or covalently bound guests, we investigated oligo(phenylene vinylene) stars with spacer-linked fullerenes and sterically crowded stars, with either hydrogen bonded guests or covalently attached pseudo guests.[26–32] The free intrinsic space between the arms was essential for the structure formation.[32] In neat star mesogens, this free space is compensated for by extremely dense packing and dimer formation.[26] If fullerene guests are introduced, they adopt the free space and double- or triple-nanosegregate into fullerene/oligo(phenylene vinylene) or fullerene/oligo (phenylene vinylene)/phthalocyanine structures, similar to conductive salts.[23,26–28] Double nanosegregation has also been observed for a crowded star with anthracene guests.[30] It undergoes a transition from a mobile columnar LC phase into a soft crystal, in which the conjugated arms are segregated from the anthracene guests in a cable-like structure with six alternating segments. Furthermore, shape-persistent stars can be considered as the basic core structure of dendrimers, which were discussed and demonstrated to be nano-containers for guest molecules.[33] Analogous to the present stars, permanent voids (core-shell structure) could only be demonstrated for shape-persistent dendrimers.[33–35]

[a] M. Lambov, N. Hensiek, Prof. Dr. A.-C. Pöppler, Prof. Dr. M. Lehmann
Institute of Organic Chemistry
University of Würzburg
Am Hubland, 97074 Würzburg (Germany)
E-mail: ann-christin.poeppler@uni-wuerzburg.de
matthias.lehmann@uni-wuerzburg.de
[b] Prof. Dr. M. Lehmann
Center for Nanosystems Chemistry
and Bavarian Polymer Institute
Theodor-Boveri-Weg 4
97074 Würzburg (Germany)

Supporting information for this article is available on the WWW under https://doi.org/10.1002/cplu.202000341

This article is part of a Special Collection on "Supramolecular Chemistry: Young Talents and their Mentors". More articles can be found under https://onlinelibrary.wiley.com/doi/toc/10.1002/(ISSN)2192-6506.Supramolecular-Chemistry.

Therefore, we became interested in whether shape-persistent star mesogens can take up the small trinitrofluorenone molecules stabilized by CT interactions in the LC phases. The present contribution investigates shape-persistent star mesogens based on the 1,3,5-substituted benzene core **1**, **2** and either oligo(phenylene vinylene)[26] or oligothiophene arms (Figure 1). The TNF mixtures are studied in solution as well as for 1:1, 1:2 and 1:3 mixtures in the solid state. These materials were subjected to a detailed structural analysis using X-ray scattering (XRS) and solid-state NMR. While XRS is one of the key techniques in the analysis of liquid-crystalline materials, the sensitivity of solid-state NMR to intra- and intermolecular proximities as well as dynamics makes the two techniques highly complementary probing long- and short-range order, respectively, for a broad range of materials[36,37] and liquid crystals in particular.[25,38,39] We found that while in solution the acceptors on average interact with the most planar centre of the star to form weak donor-acceptor complexes, they fill the space between the arms in the solid state. Neighbouring D/A-mesogens are rotationally displaced to generate CT complexes. In the time frame of our studies we could not observe a transition to a side-by-side double nanosegregation, which would be desired for a donor-acceptor conducting material. Here we highlight, that these star mesogens are liquid-crystalline nano-reservoirs for up to three guest molecules per LC-host in the columnar structures.

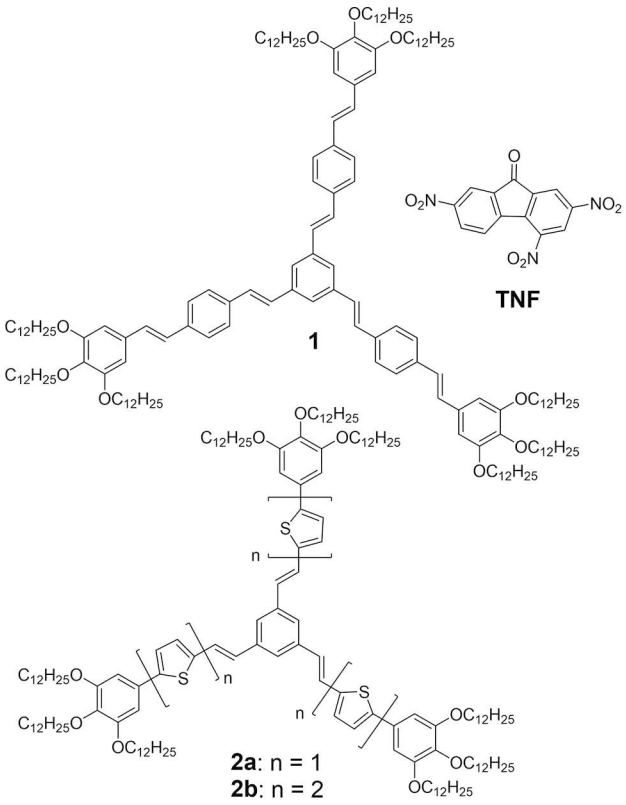

Figure 1. Shape-persistent star mesogens **1**, **2a** and **2b** and the guest 2,5,7-trinitrofluorenone (TNF).

Results and Discussion

Synthesis

Star-shaped oligo(phenylene vinylene) **1** has been synthesized according to previously described procedures.[26,40,41] The shape-persistent oligothiophene derivatives were prepared via a convergent strategy using a threefold Wittig-Horner condensation reaction of trisphosphonate **6** with aldehyde arms **5a**,**b** yielding all-(*E*) configured target molecules **2a**,**b** (Scheme 1). The aldehydes were obtained via a Suzuki reaction of boronic acid derivative **4** with the known carbaldehyde substituted bromo(oligothiophene) derivatives **3a**,**b**.[42]

The purity and identity of all derivatives have been analysed by the standard analytical investigation such as ^{1}H and ^{13}C NMR spectroscopy, mass spectrometry and elemental analysis.

Matthias Lehmann is Professor for Soft Organic Materials and Liquid Crystals at the University of Würzburg. After studies in Chemistry (University of Mainz) and postdoctoral positions at the University of Zaragoza and the Free University of Brussels, he started his independent career at the Chemnitz University of Technology. His research interests focus on synthesis, self-assembly, and application of complex soft matter with liquid-crystalline properties as new emerging materials, with an emphasis on comprehensive structural investigations by X-ray scattering, modeling, and simulation.

Ann-Christin Pöppler trained as a chemist and carried out her PhD in inorganic chemistry. She was introduced to solid-state NMR through her postdoctoral work. After stays at the MPI for Biophysical Chemistry (Göttingen) and Warwick University (UK), she started her own research group as a Junior Professor for Organic Structural Chemistry in Würzburg. Apart from sitting at the spectrometer, Ann-Christin very much enjoys teaching and training of students both in the lecture hall as well as in her workgroup.
Interdisciplinary mentoring is multifaceted. The support of Prof. Lehmann was a huge gain with respect to his profound expertise with complementary analytical tools and provided a defined space to also learn new things about my own technique. It was very motivating to learn from and with each other during this project.

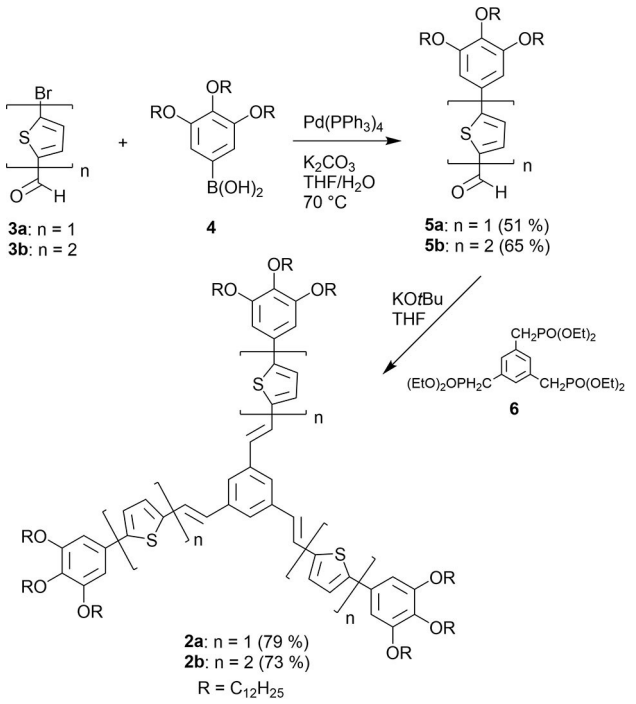

Scheme 1. Synthesis of the target molecules **2a** and **2b**.

Donor-acceptor interaction in solution and in the thin film

The interactions of TNF with the star mesogens were first investigated by UV-Vis spectroscopy in solution and thin films. While the solutions and the solids of the neat samples are slightly yellow and the solution of the mixtures with TNF showed almost no visible change in colour, the solid mixtures are dark green. The UV-Vis spectra in $CHCl_3$ (Figure S8, Table S1 in the Supporting Information) of compounds **1**–**2a**,**b**, TNF and the 1:3 mixtures of the star mesogens with TNF confirm that the absorptions are essentially superpositions of the single components. The HOMO-LUMO, π-π* transitions at 375 nm (**1**), 386 nm (**2a**) and 422 nm (**2b**) highlight the increasing conjugation of the shape-persistent arms. Magnification of the long wavelength range reveals very weak broad absorptions pointing to CT complexes, which is most pronounced for the combination of compound **2b** with TNF. In order to rationalize this observation, we performed DFT structure optimizations and calculated the HOMO-LUMO bandgaps (see ESI, Table S4). These decreased from 3.279 eV (378 nm, **2a**), 3.236 eV (383 nm, **1**) to 2.965 eV (418 nm, **2b**). Although, the sizes of the bandgaps for compound **1** and **2a** are reversed compared to the position of the absorption maxima, these results are in good agreement with the experimental values. The strongest CT complex should be expected for **2b**/TNF when comparing the calculated HOMO levels of the stars and the LUMO energy of TNF. Indeed, in solution this combination exhibits the largest effect (Figure S9, S10). Although the visual dark green appearance of the solid mixture is indicative of a CT complex due to the permanent proximity of donors and acceptors, the absorption spectrum of a thin film of the 1:3 mixture between TNF and compound **2b** shows only a weak increase in absorption in the long wave length range (Figure 2). The study of the absorption spectra of a shear aligned sample using polarized light evidences that the π-π* transition is polarized orthogonal to the shearing direction, while the weak long wavelength absorption attributed to the charge transfer absorption is polarized in the direction of the column axis (Figure 2). This is in line with the observation of Ringsdorf and Wendorff that the CT transition of the sandwiched TNF in the columnar phase of the discotic mesogen triphenylene is polarized along the column direction.[8] Consequently, in the present system, TNF takes a position within the structure, in which it also seems to be sandwiched.

Additional isothermal ^{1}H NMR titration experiments of the stars **2a** and **2b** demonstrate that all aromatic protons shift to lower ppm values (Figures S9, S10), which can be explained by the anisotropy effect of TNF. Interestingly, the changes in chemical shifts vary for the different sites, pointing at different interactions. However, the central aromatic and olefinic protons experience the largest shift upon complexation. This may be attributed to the fact that the core is the largest planar area without steric congestion (see yellow circle in Figure S9, S10) and indicates that in a time average TNF is closest to this part of the molecule. On the basis of a 1:1 stoichiometry a binding constant can be calculated by non-linear curve fitting. For a defined complex the calculation for different protons should result in the same binding constant. However, in the present case the binding constants calculated on the basis of the chemical shift of different protons decrease from the core to the periphery from $K_{11}^{core} = 26.6 \pm 1.8\ M^{-1}$ ($\Delta G_{11}^{core} = -8.1 \pm 0.2$ kJ/mol) to $K_{11}^{peri} = 17.2 \pm 1.6\ M^{-1}$ ($\Delta G_{11}^{peri} = -7.0 \pm 0.2$ kJ/mol) for **2a** and $K_{11}^{core} = 20.0 \pm 0.9\ M^{-1}$ ($\Delta G_{11}^{core} = -7.4 \pm 0.1$ kJ/mol) to $K_{11}^{peri} = 10.9 \pm 0.7\ M^{-1}$ ($\Delta G_{11}^{peri} = -5.9 \pm 0.2$ kJ/mol) for **2b**. This first confirms that the binding constants are extremely low, secondly that there is not a rigorously defined complex structure and thirdly that the preferred position for TNF

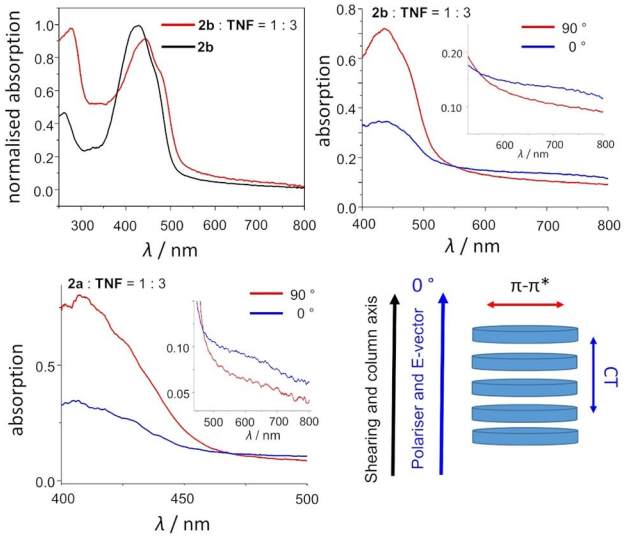

Figure 2. UV-Vis-spectra and polarized UV-Vis absorption spectra in thin films and sheared, i.e. oriented thin films.

interaction in solution seems to be the core of the star mesogens.

Thermotropic properties

Information about the interaction and self-assembly of guests and hosts in the solid state can be obtained by the investigation of the thermotropic properties. They were first studied by polarized optical microscopy (POM) and differential scanning calorimetry (DSC). The results are shown in Figure 3 and the data is collected in Table 1.

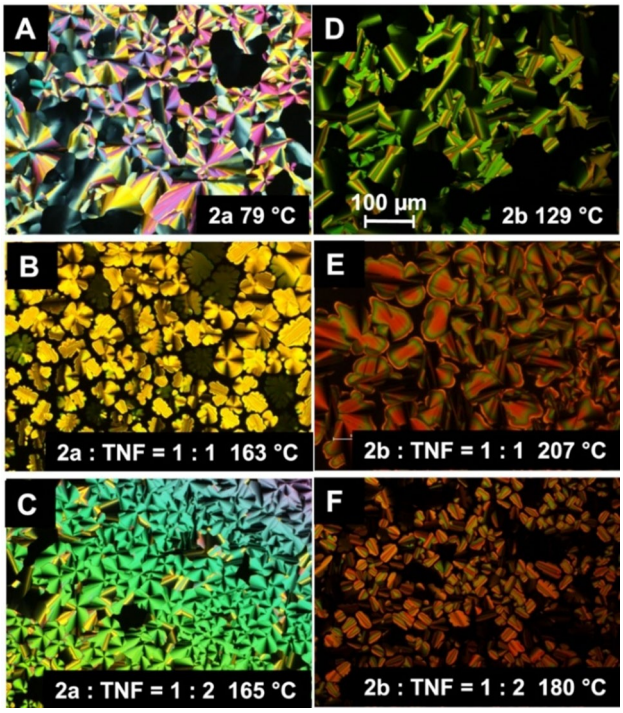

Figure 3. Selected POM textures of the neat compounds **2a**, **2b** and their 1:1 and 1:2 mixtures between crossed polarisers.

Table 1. Thermotropic properties by DSC and POM.

Compound	transition temperature in °C Onset [Peak]/transition enthalpy [kJ/mol][a,b]
1	Col_h 108/4.0 I
1:TNF = 1:1	Col_{hH} 111.3/3.7 Col_h 154.1 (175.0)/2.3 I
1:TNF = 1:2	Col_h 204.0 (225.2)/23.6 I
1:TNF = 1:3	Cr_{soft} (Col_{ob}) 77.9/4.6 Col_h 221.5(235.7)/27.8 I
2a	Cr 62.8/59.2 Col_h 90.6/4.1 I
2a:TNF = 1:1	Col_{hH}–Col_h 171.8(182.7)/10.7 I
2a:TNF = 1:2	Col_{hH}–Col_{h1} 151.9/9.0 Col_{h2} 170.7 (183.5)/9.2 I
2a:TNF = 1:3	Col_{hH}–Col_{h1} 149.7/11.0 Col_{h2} 170.9 (180.5)/ 9.8 I
2b	Col_{hH}–Col_h 128.5 (136.8)/2.9 I
2b:TNF = 1:1	Cr_{soft} (Col_r) 95.1/2.6 Col_h 191.1 (207.3)/7.7 I
2b:TNF = 1:2	Cr_{soft} (Col_r) 105.4/5.3 Col_h 228.4 (238.1)/18.9 I
2b:TNF = 1:3	Cr_{soft} (Col_r)104.2/3.2 Col_h 234.7 (244.7)/30.4 I

[a] Col columnar LC phase, h hexagonal, h1 hexagonal with higher inter columnar correlation than h2, H helical, r rectangular, ob oblique, Cr_{soft} soft crystal, i.e. CONDIS crystal (conformational disordered), Cr crystal, I isotropic liquid. [b] In general the heating rate was 10 °C/min. In cases, in which the transitions could not be detected, higher heating rates were chosen (20 °C/min for **2b**:TNF = 1:2 and 1:3 and 40 °C/min for **1**:TNF = 1:1 and 1:3, **2b** and **2b**:TNF = 1:1. Irrespective of the rates, the transitions of the mixtures are rather broad ($T_{Cl,peak}$–$T_{Cl,onset}$ = 14–23 °C (**1**), 10–13 °C (**2a**), 10–17 °C (**2b**), which can be attributed to the statistical distribution of the TNF in the LC mixtures.

The neat compounds **1**,[26] **2a** and **2b** self-assemble into liquid-crystalline phases with pseudo-focal-conic, mosaic and homeotropic textures pointing to Col_h phases at high temperatures. The clearing temperatures T_{cl} increase with the size of the mesogens **2a** (r_{core} = 12.6 Å, T_{cl} = 90.6 °C), **1** (r_{core} = 16.2 Å, T_{cl} = 108.0 °C), **2b** (r_{core} = 16.8 Å, T_{cl} = 128.5 °C) (compare Figure 6). The formation of mesophases with the TNF guest was first tested with contact samples for compounds **2a** and **2b** (Figures S11, S13). They exhibit a tremendous increase in clearing temperatures by up to 113 °C (Table 1). The most stable mixtures were formed close to the TNF phase with rather high TNF content. Thus, 1:1, 1:2 and 1:3 star mesogen/TNF mixtures have been prepared. While the larger stars **1** and **2b** reveal the expected increase in stability with increasing TNF content, the mixtures **2a**/TNF show almost similar stabilities with a slightly higher clearing temperature for the 1:1 mixture. The behaviour of compounds **1** and **2b** can be explained by the stepwise filling of the intrinsic free space accompanied by an increasing transition enthalpy and entropy at the clearing point (order-disorder transition). This is rationalized by the increasing quantity of attractive interactions between TNFs and the donor star molecules in the liquid crystal (enthalpy) and the larger number of building blocks when the LC phase melts to the isotropic liquid (entropy).

The smallest star **2a** exhibits an exceptional behaviour. The 1:1 mixture displays a smooth DSC curve with only one transition at 171.8 °C and a rather high transition enthalpy of 10.7 kJ/mol. Adding TNF did neither significantly change the transition temperature nor the transition enthalpy or entropy. A further very broad signal appeared in the DSC curves of the 1:2 and 1:3 mixtures extending approximately from 125 to 165 °C and corresponding to an increase in the transition enthalpy from 9.0 kJ/mol to 11.0 kJ/mol. This transition is not visible in the POM studies and consequently, it is not related to a change in the overall structure of the mesophase. X-ray studies indicate that the high intercolumnar order (see next section) is lost at this transition, while the hexagonal structure is maintained. Thus, the present result is a complex interplay of enthalpy (charge transfer interactions and maximizing space-filling i.e. van der Waals interactions) and entropy (number of particles, conformation, intra- and intercolumnar order) contributions, as was observed for other supramolecular systems.[27,29,43]

At lower temperature, below 110 °C, the materials become highly viscous and develop crystalline, soft-crystalline or columnar phases of lower symmetry, which could be only discovered by X-ray scattering methods.

X-ray studies and modelling

For the temperature-dependent X-ray scattering studies all materials were extruded to a fibre from the liquid-crystalline state to produce aligned materials.

Figure 4 shows the results of the integrated patterns along the equator and the meridian at selected temperatures in the LC phases. The equatorial reflections can all be indexed according to columnar hexagonal phases. The corresponding *a* parameters are listed in Table 2. The neat materials show no π-π interaction evidenced by the missing wide angle signal corresponding to a distance between 3.4–3.6 Å. For compound **1**, it was recently highlighted that it arranges in a dense helical self-assembly with a helical pitch of 38 Å and 1.8 molecules per columnar unit of 3.4 Å height (typical π-π distance for comparison), based on a set of diffuse meridional signals at room temperature.[27] The neat smaller star **2a** does not exhibit any of these weak meridional signals in the hexagonal phase, but it transforms to a soft crystalline phase (Figure 5A), for which the number of molecules Z′ per columnar repeating unit of 3.4 Å can be calculated based on the experimental density to be 1.5 at 25 °C. This decreases to 1.2 in the hexagonal phase at 75 °C (Table 2). In both phases, the number of molecules per columnar slice of 3.4 Å height is larger than one molecule, which is a direct sign of the free intrinsic space in a single mesogen, which is filled by other neighbouring molecules in the liquid-crystalline material. The smaller number compared to **1** reflects the smaller size of the star **2a** and the corresponding intrinsic void. Compound **2b** with a slightly larger size compared with **1** assembles with 1.9 molecules per 3.4 Å and clearly exhibits meridional signals growing in at 25 °C pointing to a helical arrangement with a helical pitch of 48 Å (see Figure 5B). In general, the need of efficient space-filling leads to soft crystals for smaller stars and to dense helical packing for the larger shape-persistent star mesogens.[26,27,44]

TNF should fill these voids promoted by the favourable charge transfer interaction within the columnar stack, which is evidenced by the UV-Vis absorption spectroscopy in thin solid films. Figure 4 clearly reveals that no signs of crystalline TNF are detected for any of the mixtures indicating that TNF forms new phases with the star mesogens without macroscopic separation. However, an excess of TNF over the 1:3 ratio, for example in 1:4 and 1:6 mixtures studied for compound **2b** in the LC phase below the melting temperature of TNF revealed crystalline TNF portions, indicating that not more than one TNF is incorporated into the individual void between the arms (Figure S33). The 2θ scans in the LC phases unravel important details for the materials as a function of increasing TNF content (Figure 4, Table 2): (i) The 2D arrangement of the columns gets more defined since the higher order reflections (11, 20, 21, 30, 31) become more intense and clearly visible for all 1:3 mixtures; (ii) The intercolumnar distances (*a* parameters) continuously decrease for the larger stars with increasing TNF fraction (**1**: 47.4 Å (0 mol% TNF) to 44.3 Å (75 mol% TNF); **2b**: 47.9 Å (0 mol% TNF) to 44.7 Å (75 mol% TNF)) and is constant for the small star (**2a**: 40.5 Å (0 mol% TNF) to 40.7 Å (75 mol% TNF)) (Table 2); (iii) besides the halo corresponding to the average distance of the liquid-like aliphatic chains, two signals are growing in at about 3.5 Å and 3.4 Å and the latter gain enormously in intensity for the 1:3 mixtures; (iv) For the 1:3 mixtures, there is additional diffuse intensity at approximately

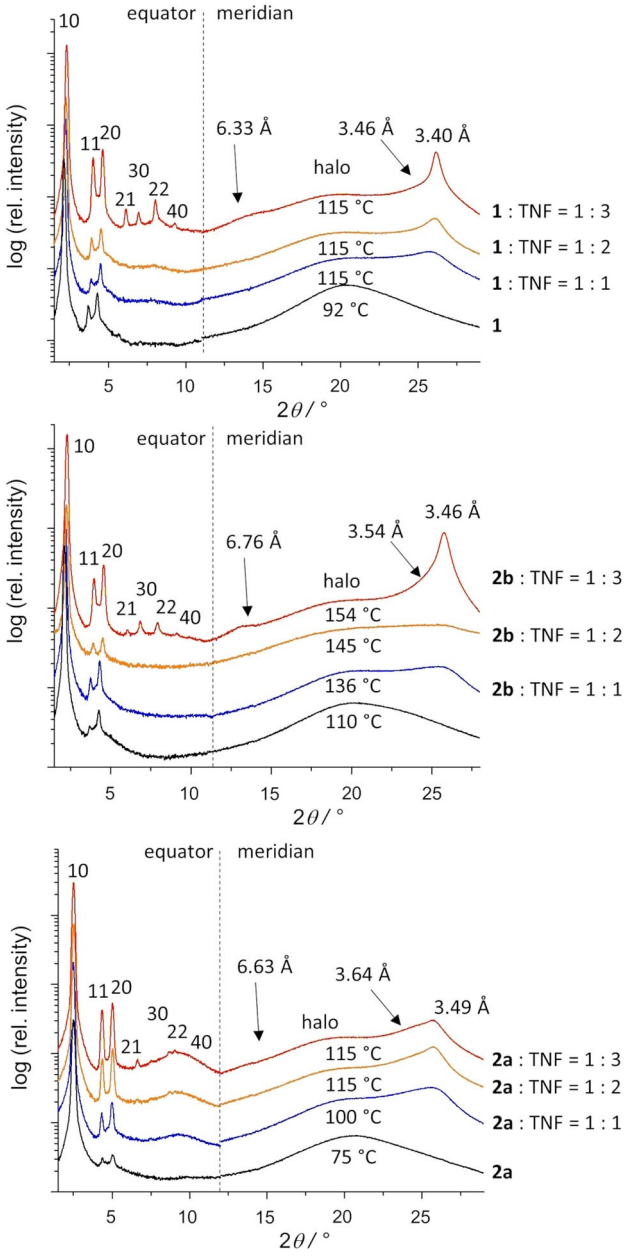

Figure 4. 2θ-scans along the equator and meridian of X-ray scattering patterns of aligned fibres taken in the hexagonal columnar phase of **1**, **2a**, **2b** and their 1:1, 1:2 and 1:3 mixtures with TNF.

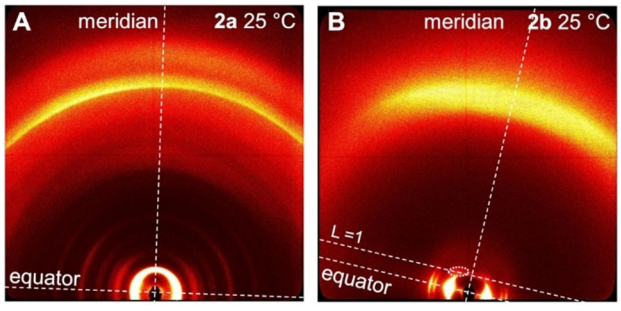

Figure 5. XRS pattern of **2a** and **2b** at 25 °C. Left: Soft crystalline phase of **2a**. Right: Helical columnar hexagonal phase of **2b**.

Table 2. Unit cell parameters, density, molecular volume and number of molecules per columnar slice of 3.4 Å height.

Compound	T/°C	*a*, *b* (*c*; hp[a]) [Å] γ [°]	ρ [g cm^{-3}][b]	V_M [Å^3] [c]	Z' per 3.4 Å [d]
1	30	49.7 (–; 38)	0.960[f]	4064	1.79
	100	47.4			
1:TNF = 1:1	80	46.1 (–; 65.7)	–	–	–
	115	45.4 (3.4; –)			
1:TNF = 1:2	115	45.3 (3.4; –)	–	–	–
1:TNF = 1:3	25	44.9, 36.2, γ = 58°, (7.32; –)	1.083	5052	0.93
	115	44.3 (3.4; –)	1.034[e]	5294[e]	1.092
2a	25	75.3, 47.1	0.973	3907	1.54
	75	40.5	0.942[e]	4034[e]	1.17
2a:TNF = 1:1	25	43.5 (–; 49.6)	1.045	4139	1.34
	110	41.0	0,991[e]	4365[e]	1.13
2a:TNF = 1:2	25	40.3 (–; 59.2)	1.054[g]	4602	1.04
	115	40.5	1.000[e]	4845[e]	1.00
2a:TNF = 1:3	25	40.5 (–; 60.0)	1.125	4775	1.01
	115	40.7 (6.5; –)	1.071[e]	5016[e]	0.97
2b	25	51.4 (–; 49.5)	1.021	4124	1.88
	100	47.9			
2b:TNF = 1:1	25	74.4, 43.6 (7.6; –)	1.069	4429	1.25
	136	47.3	1.000[e]	4735[e]	1.39
2b:TNF = 1:2	25	75.3, 43.1, (7.6; –)	–	–	–
	145	45.1			
2b:TNF = 1:3	25	66.2, 41.0 (7.7; –)	1.115	5185	0.89
	154	44.7 (7.0; –)	1.041[e]	5883[e]	1.06

[a] *hp* helical pitch and repeat of the helix; [b] density obtained by the buoyancy method; [c] molecular volume calculated by $V_m = M/(\sigma^* N_A)$; N_A = Avogadro's constant; [d] number of molecules Z' filling a columnar slice of 3.4 Å height calculated for the indicated density. The 3.4 Å correspond to the typical π-π-distance of the D–A complex and has been chosen for comparison; the number Z of molecules in the complete unit cell can be calculated by $Z = Z'c/3.4$ Å or alternatively by $Z = Z'hp/3.4$ Å. [e] At higher temperature no density data could be measured. The density has been estimated assuming that there is only a significant volume change of the aliphatic chains. This can be calculated according to reference [45] The molecular volume $V_{m,T}$ is then calculated as the sum of the molecular volume V_m at 25 °C and the volume change of the aliphatic chains. The density is subsequently obtained by $\sigma = M/(V_{m,T}{}^* N_A)$, [f] density from reference [27]; [g] calculated X-ray density.

the double π-π-distance (6.3–6.8 Å); (v) There is also a diffuse signal increasing in intensity on the equator corresponding to approximately 9.5 Å (**2a**) and 11–12 Å (**1**, **2b**). The increasing order and decreasing or constant intercolumnar distance can be explained by the incorporation of TNF into the free intrinsic space between the arms of the stars. In the neat materials the stars have to arrange by translational, rotational displacement from the column centre and additional torsional deformation.[26] At room temperature, this leads to a helical packing with low correlation length, thus, it is still rather disordered. TNF fills the free space (cp. Figure 6). Consequently, the number of star molecules Z′ per columnar slice (table 2) decreases. Since TNF itself does not possess flexible chains, its incorporation reduces the number of aliphatic chains in the periphery of the columns. Subsequently, their packing by folding and interdigitation results in a decrease of the intercolumnar distance.

In case of **2a**, the void is rather limited, and TNF juts out over the limit of the aromatic part of the star and consequently also occupies space previously filled by the aliphatic chains and therefore, the diameter remains almost constant. The signals at wide angles can only be fitted with two different π-π distances, which may arise from donor-acceptor interactions (star-TNF), star-star contacts and TNF-TNF stacks. Since TNF π-stacking was reported in a dense crystal to be approximately 4 Å,[46] while the donor-acceptor stack between TNF and hexamethylbenzene is only separated by 3.35 Å,[47] it is more reasonable to attribute the shortest distance to the donor-acceptor separation. The very diffuse liquid-like signals, exclusively on the equator and especially intense for the small star **2a**, are unique and correspond to distances much shorter than the intercolumnar distance. We attribute them to lateral TNF-TNF distances within columns, which are more defined in the cavities of the small star and less well defined in the larger cavities (see Figure 6).

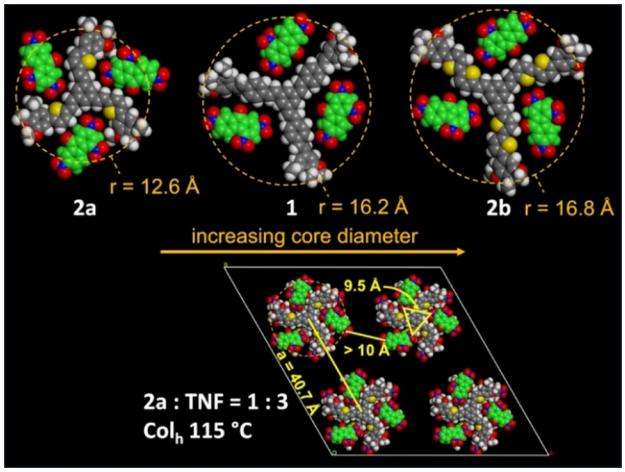

Figure 6. Models of the compounds with a methoxy periphery instead of the long alkoxy chains for clarity. Top: Models of compounds **1**, **2a** and **2b** with three TNFs filling the intrinsic free space between the conjugated arms. For **2a** the TNF guests extend slightly over the size of the radius of the aromatic scaffold. Bottom: Supercell (four cells with a = 40.7 Å) of the 1:3 mixture of **2a** with TNF rationalizing the different distances found at the equator of the diffraction pattern.

The very weak additional meridional signals at approximately the double π-π distances for the 1:3 mixtures indicate that an alternating packing along the column plays a role; this might be like a sandwich when the rotational displacement is 60°, but also smaller intermediate angles are feasible, which might be the beginning of a helical packing.

More detailed information can be extracted from the soft crystal structures at room temperature. Soft crystals for complex column-forming mesogens often remain in the columnar self-assembly and the positional and/or orientational order along a single column or even between columns increases.[48,49] Owing to the still existing conformational disorder of the peripheral aliphatic chains or the more anisometric cores and the low correlation lengths, the materials possess a soft nature and are also called conformational disordered crystals (CONDIS crystals).[50] In the series of mixtures more ordered phases are generated below 100 °C – either helically ordered hexagonal phases (Col_{hH}) or soft crystal phases with columnar rectangular or oblique order (Tables 1 and 2). In the following section, we focus on the mixtures of compounds **2a** and **2b**, since the low temperature phases at 25 °C keep structures of higher symmetry compared to compound **1**. It should be emphasized that from the data, only information about the columnar topology and nearest neighbours can be obtained. The soft structures of the 1:1 and 1:3 mixtures of **2a** with TNF gain additional positional order along the *c*-axes of the columns at 25 °C compared to the high temperature phase, but continue to be in the hexagonal columnar two-dimensional packing (Figure 7A). The diffuse small angle signals point to large periodicities, which can be best explained by helical stacks of the molecules. For the 1:1 mixture, the most intense signals are attributed to the layer lines L = 2 and 4, which points to the formation of a double helix with a repeat and helical pitch of 49.6 Å. Density measurements (Table 2) demonstrate that the number of molecules in the unit cell is Z = 20, thus more than one complex fills a columnar slice of 3.4 Å height. Therefore, two neighbours along the *c*-axis are rotated by 60° and shifted radially in order to avoid the steric repulsion of the cores in the centre of the column (Figure 8A, two filled yellow circles). The two guest molecules are packed in two opposite pockets of the stars (Figure 8 A) and the whole dimer is rotated by 36° (360°/10 dimers) along the *c*-axis to generate the helix (Figure 8B). This model was geometry optimized with the program Materials Studio (Forcite) obtaining large negative non-bonding (van der Waals/electrostatic) interactions demonstrating the stability of the assembly (see ESI). Fibre X-ray scattering simulation with the program Clearer,[51] confirms the consistency with the main features in the experimental pattern and further supports the packing model (see ESI).

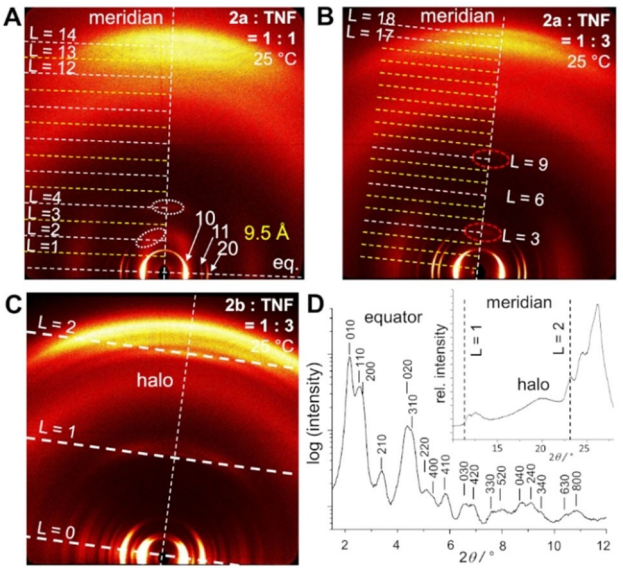

Figure 7. X-ray patterns of the highly ordered phases of the 1:1 (A) and 1:3 (B) complexes of **2a** and the 1:3 complex of **2b** with TNF (C,D).

The model of the 1:1 mixture implies that the TNF guests are located in a sandwich-like position between the conjugated arms of the star. TNF fills only one of the three pockets, thus the other two intrinsic free spaces have to be filled by the star mesogen and therefore a shift of the core from the central position is necessary. This changes for the 1:3 complex between **2a** and TNF. The XRS pattern is consistent with a hexagonal columnar phase and the diffuse signal at the third layer line (L = 3) corresponds to a triple helix of 60 Å (helical pitch, *hp*) (Figure 7B). The experimental density agrees with *Z* = 18 mesogens in the helical repeat unit and thus with one complex per 3.3 Å. Consequently, the centre of the star can be located again at the centre of the column (Figure 8C). In principle, the TNF-filled star can be arranged differently with respect to the next neighbours in the helix, but it turned out that the best agreement between the simulated and experimental diffraction pattern (Figure S37) is obtained when two neighbours are rotated by 60° to first form a dimer, in which the donor-acceptor interactions are optimized (Figure 8C). This dimer is then helically assembled by rotation of 40° (360°/9 dimers) about the column axis (Figure 8D). From this analysis and the geometry optimized models, it is reasonable that the guest molecules occupy the pockets of the star mesogens and that the most important stacking along the column is realized by a donor-acceptor contact in dimers. However, rotational displacements render also TNF-TNF and star-star stacks possible and certainly increase in number in the more disordered liquid crystals leading to an additional π-stacking signal.

These packing motifs are further supported by the structure of the 1:3 complex of **2b** with TNF. At room temperature a new columnar phase forms, in which the hexagonal symmetry is broken owing to the higher ordered assembly of the complexes (Figure 7C,D). The equatorial reflection can be attributed to a rectangular phase of p2 mg symmetry with the systematic absence of the reflections h00 with h = 2n + 1. The meridional reflections with a maximum at 6.66 Å point to an alternating stacking along the *c*-axis. The symmetrical restrictions can only be explained by mesogens tilted along the *b*-axis as shown in Figures 8E,F. Although this model exhibits a quasi-C_3-symmetric mesogen, in which the thiophene sulphur points always to the same side, a distribution of different conformers is certainly present in the real structure. In this case the star molecule averages to be symmetric with respect to a mirror plane in a

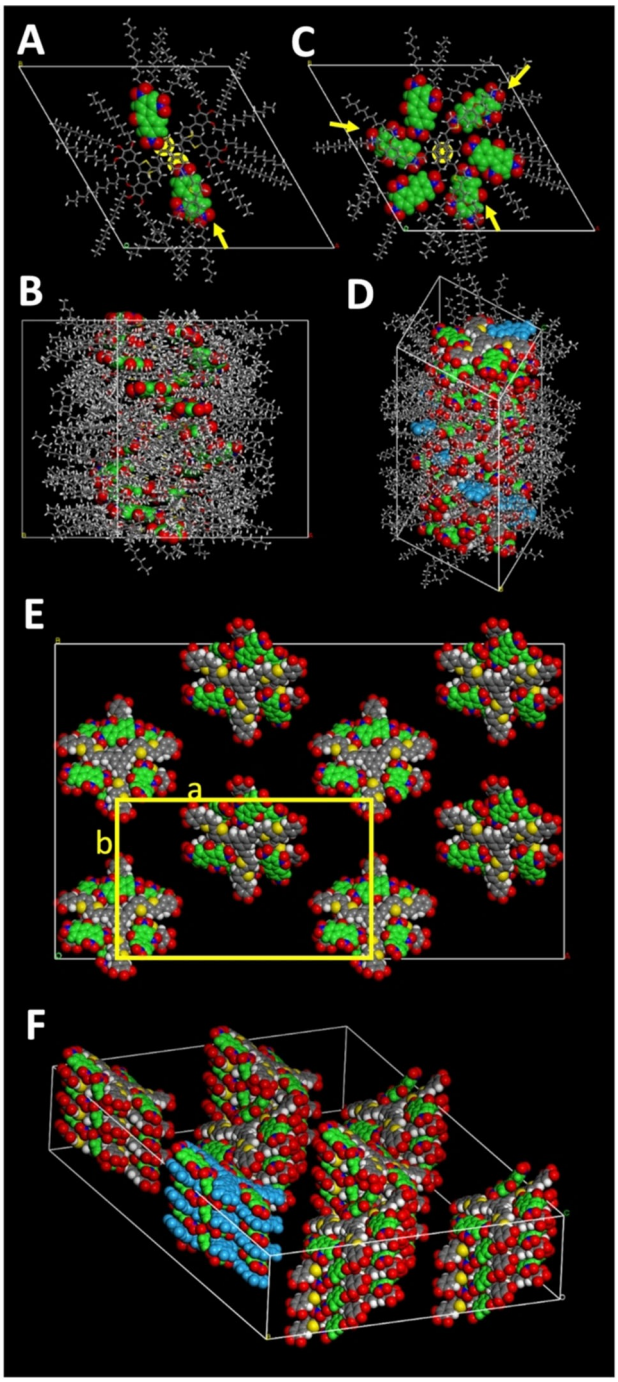

Figure 8. Models of the soft crystalline phases (TNF in green). A: Dimer of the **2a**:TNF 1:1 complex shifted with the molecular centres (yellow circles) from the columnar centre. B: Double helix formed from dimer in (A) by rotation of 36° along the columnar axis. C: Dimer of the **2a**:TNF 1:3 complex with the molecular centres (yellow circles) both in the middle of the column. The two 1:3 complexes are rotated by 60° to each other. Yellow arrows indicate the arms on top of TNFs. D: Helix generated by the dimer of (C) by Rotation of 40° along the columnar axis. E, F: Supercell of the soft crystal ($Pmn2_1$) of the 1:3 complex of **2b** with TNF. The TNF guests are sandwiched between the oligothiophene arms (highlighted in one stack in blue).

planar group of p2 mg symmetry, when one arm is located in the mirror plane and the molecule is tilted along this direction. In order to keep this symmetry, the next complex mesogen along the column axis has to be rotated by 60°. This symmetry strictly prefers the sandwich structure of the TNF and explains the signal at the first layer line corresponding to a distance of 6.66 Å (Figure 7C,D). In conclusion, the complete structure in three dimensions can be described by the space group $Pmn2_1$ assuming a symmetric star scaffold either by motional averaging or by a corresponding equal distribution of conformers.

Solid-State NMR Study

Due to the sensitivity of NMR with respect to short-range order phenomena, subtle changes in packing and intermolecular interactions, the samples were also subjected to a series of solid-state NMR experiments at moderate magic angle spinning (MAS) rates. To ensure that the soft materials did not undergo changes as a consequence of the forces resulting from spinning the samples, all measurements were done at 280 K to compensate for frictional heating and ^{1}H NMR experiments before, during and after the measurement were recorded, which proof that the samples are stable during sample rotation for 1–2 days (Figure S38).

In a first step, the ^{13}C CP MAS NMR spectra of **2a** as well as a 1:1 and 1:3 mixture of **2a** with TNF are compared (Figure 9). To account for the very high intensity of the aliphatic chains, the spectra are represented in two parts with the spectral region between 60 and 200 ppm displayed with eight times higher intensity compared to the region below 50 ppm. In a first step, ^{13}C NMR signal assignment was done using the data

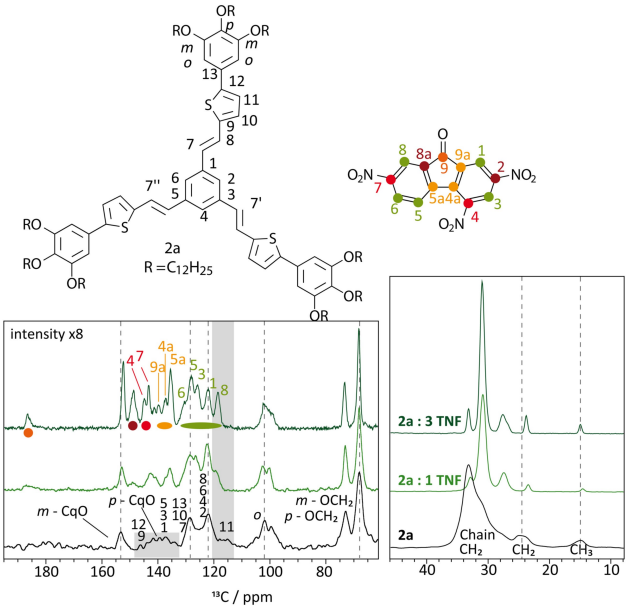

Figure 9. Molecular structures and the numbering as well as colour scheme used for assignment alongside ^{13}C CP MAS NMR spectra of **2a** (black) and the 1:1 and 1:3 mixture of **2a** with TNF(light and dark green). For better comparison of the datasets, the spectra were divided into two spectral regions with the left extract displayed with an eightfold increased intensity. All spectra were recorded at 14.1 T and 12.5 kHz MAS with sample cooling to 280 K. 11000 (**2a**) and 3600 (mixtures) individual scans were recorded with a recycling delay of 3 s.

for pure **2a** (black) alongside 2D ^{1}H–^{13}C HETCOR data with short contact times of 0.05 ms to identify carbons with hydrogen atoms attached to them. This was complemented by quantum chemical calculations of an X-ray based model structure of **2a** with shortened aliphatic chains (Chapter S14 of the SI). Overall, the calculations agree very well with the experimental data correctly predicting various features such as the distribution of different chemical shifts around 140 ppm (grey box) and the two inequivalent sites found for the *ortho*-CH moiety (o) of the outer aromatic rings. For the assignment of the TNF resonances, the mixture with the highest TNF content was used, which at the same time is also the sample yielding the most well-defined spectrum (dark green). The numbering scheme and signal assignment is in agreement with previous data from the literature.[52,53] A full assignment including a numbering scheme for the two components is shown in Figure 9.

Comparing the three datasets shown in Figure 9, several interesting features can be discussed: (i) With increasing TNF content, the spectra show narrower signals both for the aliphatic chains and for the moieties at higher ppm values. Two features can be discussed in this context, mobility and the degree of order. The former was supported by ^{13}C NMR using direct excitation (DE) and very short relaxation delays of 0.8 s (Figure S39) showcasing the mobility of the aliphatic chains in the order **2a** ≪ 1:1 > 1:3 mixture. This shows a denser structure within the chain nanophase for neat **2a** compared to the mixtures with TNF (see also references [6,9]) and thus less mobility of the aliphatic chains and is in agreement with the structural model derived from the X-ray data in Table 2: Upon addition of TNF, the fraction of chains per columnar slice of defined height decreases. Interestingly, a change in the chemical shift of the majority of CH_2 groups from ca. 33 to 31 ppm can be observed. (ii) All other parts of the molecule are more rigid and thus, order phenomena need to be included in the discussion. The distribution of chemical shifts in specific areas of the spectrum of **2a**, highlighted by grey boxes is no longer observed in the mixtures with TNF. This effect is most dominant for C11 at the thiophene moiety. Instead of the broad distribution of signals from 113 to 123 ppm, a clean signal at 119 ppm is observed for C11 overlapping with C8 of TNF. This shows that the chemical environment of the thiophene is more defined in the presence of TNF. (iii) A similar although less drastic effect is also observed for the signal of the *m*-CqO atoms at the outer ring, which also shifts to lower ppm values upon increasing the TNF content. (iv) Finally, while the signal of the first OCH_2 group of the aliphatic chain is unaffected by the presence of TNF, the aromatic *o*-CH unit at the outer ring is showing an interesting behaviour: In pure **2a**, there are two environments for the two sides of the aromatic ring (CH on the "sulphur" side and CH on the double bond side). In the 1:1 mixture, this distinction is still possible, while for the 1:3 mixture, this feature is blurred. This could indicate the presence of TNF in proximity to this moiety.

Analogous sets of experiments served to analyse the effect of an additional thiophene unit in molecule **2b**, thus yielding a more extended system with larger "bay areas" to accommodate guest molecules (Figures S38 and S40). The mobility of the alkyl chains in the 1:3 mixture of **2b** with TNF is only slightly lower than in **2a**:TNF (1:3). In the ^{13}C CP MAS experiment the main features of the spectrum are retained for the mixtures with **2a** and **2b** despite the different structures (soft columnar crystal with $Pmn2_1$ symmetry (**2b**:TNF) and Col_{hH} structure (**2a**:TNF)), thus pointing to similar local structures. CH resonances for the additional thiophene can be observed at 125 and 132 ppm. Furthermore, the environment at the *meta*-position of the outer aromatic ring is altered in the way that the quaternary carbon at 152.3 ppm shifts about 1 ppm to higher values for the larger star **2b**, while the corresponding first adjacent CH_2 chain unit (OCH_2) shows a broader distribution of environments. This less defined environment is also observed for the spectral areas around 140 and 145 ppm indicating that the addition of the second thiophene unit increases the conformational freedom yielding distributions of similar but not identical local arrangements.

To gain a deeper understanding of the intermolecular interactions of TNF with **2a** and **2b**, additional ^{1}H–^{13}C FSLG HETCOR spectra with longer contact times of 3 ms were recorded for the two mixtures with highest TNF content (Figure 10). With increasing contact time, longer-range C···H distances are also sampled, and thus also intermolecular interactions can be observed. Due to the substantial signal overlap between the aromatic moieties, interpretation in this spectral region is difficult and it is thus necessary to focus on

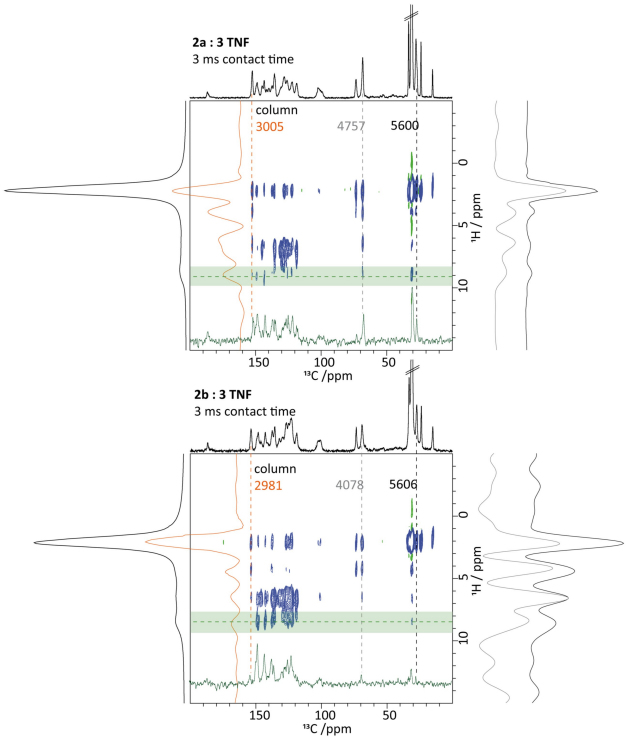

Figure 10. ^{1}H–^{13}C FSLG HETCOR spectra of the 1:3 mixtures of **2a** (top) and **2b** (bottom) with TNF using a contact time of 3 ms recorded at 12.5 kHz MAS, 280 K and 14.1 T. 228 and 204 transients were co-added for each of the 100 *t1* FIDs. Forward linear prediction of 50 additional *t1* FIDs was used to increase resolution in the ^{1}H dimension. The individual 1D NMR spectra are shown as projections of the 2D dataset and slices of important spectral rows and columns are displayed in green, orange, grey and black.

unambiguous, clearly assigned peaks to extract information on intermolecular contacts. One such area is the ^{1}H chemical shift range between 8–9 ppm (highlighted in green), which exclusively contains signals of TNF in agreement with previous reports from the literature.[38] The extracted horizontal slice at 9.1 ppm is shown in dark green. While significant spin diffusion occurs within the TNF molecule during the 3 ms contact time, signal intensity at ^{13}C carbon positions exclusively belonging to **2a** or **2b** indicates through space proximity to TNF.

For both **2a** and **2b**, intermolecular contacts to the outer aromatic ring, in particular to *m*-CqO (152/153 ppm), the aromatic *o*-CH fragment (100–102 ppm) and the connected alkyl chain resonances at 68 (OCH_2), 31 and 27 (CH_2 chain) ppm were observed. To analyse the intensity differences found for **2a** and **2b** in more detail, vertical slices at three different representative ^{13}C environments were extracted and the relative signal intensities subsequently compared. Focusing on the orange column (*m*-CqO), the contacts at low ppm values (alkyl chain) and higher values (aromatic parts) are more comparable for **2a** than for **2b** were the contacts in the area of around 2 ppm dominate. This could be a sign of an overall more closely packed arrangement in case of the smaller star-shaped molecule. An inverted situation is observed for the columns in grey and black (OCH_2 and CH_2 chain). Consequently, in the mixture of **2a** with TNF close to the aromatic moieties, interchain contacts dominate while for the mixture with **2b** the alkyl chains experience a more diverse environment due to more space in the packing and thus a larger conformational freedom in agreement with the discussion illustrated in Figure 6.

Overall, this means that the solid-state NMR measurements (i) support the findings on the degree of order as identified in the XRS experiments of the different structures and (ii) the densities of packing with the corresponding mobilities. Furthermore, (iii) the location of TNF within the pockets of the mesogens is supported by these measurements. Although there are clear contacts between TNF and the chains, a phase separation with the TNF molecules located fully within the aliphatic chains could neither account for the contacts *m*-CqO to TNF nor the increase in order for the thiophene C11 moiety. Finally, (iv) the changes in the HETCOR data between **2a** and **2b** with 3 eq. TNF also provide additional support to the molecular arrangement with the TNF molecules almost pressed into the voids between the arms and thus closer to the aromatic moieties for **2a**, while TNF in **2b** is looser and thus in less direct and close contact to the aromatic units.

Conclusion

Shape-persistent star mesogens with conjugated arms of different nature and length were successfully synthesized. They are liquid crystalline and pack densely in columnar structures with helical order at low temperature. With 2,4,7-trinitrofluorenone (TNF), these mesogens form very weak CT complexes in CD_2Cl_2, and interact preferentially with the planar core area. Although this would imply that in the mixtures the molecules form sandwich aggregates with the core, in the liquid-crystalline matter such structures are absent. All mixtures generate different columnar soft materials and possess a high temperature hexagonal columnar phase. The three intrinsic free spaces of the star-shaped mesogens can host up to three TNF molecules and indeed incorporate these guests. No macroscopically segregated TNF molecules could be detected. Compared to the neat LC materials, TNF stabilizes the mesophases by more than 100 °C and increases the inter- and intracolumnar order. The 1:3 complexes possess the highest order. At 25 °C most of the mixtures reveal either a soft crystal or a hexagonal helical columnar phase. X-ray studies complemented by solid-state NMR experiments highlight that the TNFs are sandwiched in these structures and occupy the intrinsic free space between the conjugated arms. Thus, the LC phases can be considered as endo receptors for guest molecules. This has been further confirmed by solid-state NMR probing specific through-space proximities between TNF and the star-shaped molecules via 2D correlations, while changes in the line width and distribution of chemical shifts support this picture of the TNF-star interaction as well as the increase in structural order upon going from the neat mesogens to the 1:3 mixture.

Future work will explore the utility of these LC reservoirs for different purposes such as drug storage or delivery. In this context, it will be important to study in more detail how the presence of different guest molecules influences the LC structure and properties and if and how the molecules could be released.

Experimental Section

XRS experiments: The temperature dependent WAXS investigations were performed on a Bruker Nanostar (Detector Vantec2000, Microfocus copper anode X-ray tube Incoatec). The fibres were produced by extrusion from the liquid crystal state with a homemade miniextruder. The aligned fibres were transferred to Mark capillaries, which were sealed and glued into the metal sample holder, with the fibre direction parallel to the tilt direction of the detector (tilted by 14°). The XRS heating system was calibrated by liquid crystal standard compounds. The XRS data was evaluated by the program datasqueeze using silver behenate as a calibration standard.[54] The correlation lengths were estimated with the Scherrer formula.[55]

Solid-state NMR: The data were measured using a 3.2 mm double-channel Bruker probe at 14.1 T and 12.5 kHz MAS. The temperature was lowered to 280 K to account for frictional heating during MAS. The magic angle was set using KBr, while the chemical shifts were referenced with adamantane (left signal at 38.48 ppm). For all experiments, the ^{1}H 90° pulse length duration was 2.5 μs.

For the ^{13}C NMR spectra with direct excitation, a short recycle delay of 0.8 s was used to sample predominantly mobile parts of the molecules. For ^{1}H–^{13}C cross polarization (CP), a 70 to 100% ramp on the ^{1}H channel was used for a CP contact time of 2 ms. SPINAL64 heteronuclear decoupling was applied with a pulse duration of 4.8 μs at a ^{1}H nutation frequency of 100 kHz during acquisition of the ^{13}C FID. 2D ^{1}H–^{13}C HETCOR spectra were recorded with short and longer contact times (0.05 and 3 ms) using the frequency switched Lee-Goldberg sequence to suppress ^{1}H homonuclear

coupling and the States-TPPI method to achieve sign discrimination in F_1.

Acknowledgements

We thank Marvin Grüne and Sebastian Scheidel for their support with preparation of the centre-packed MAS rotors and setting up of the solid-state NMR experiments.

Conflict of Interest

The authors declare no conflict of interest.

Keywords: donor-acceptor interactions · host-guest systems · intrinsic free space · liquid crystals · mesogens

[1] A. F. Garito, A. J. Heeger, *Acc. Chem. Res.* **1974**, *7*, 232–240.
[2] W. Pisula, K. Müllen, *Handbook of Liquid Crystals, Vol. 8: Application of Liquid Crystals Liquid Crystals*, 2nd ed. (Eds. J. W. Goodby, P. J. Collings, T. Kato, C. Tschierske, H. F. Gleeson, P. Raynes), Wiley-VCH: Weinheim **2014**, pp. 627–673.
[3] S. Günes, H. Neugebauer, N. S. Sariciftci, *Chem. Rev.* **2007**, *107*, 1324.
[4] J. Hou, O. Inganäs, R. H. Friend, F. Gao, *Nat. Mater.* **2018**, *17*, 119–128.
[5] Z. Liu, Y. Wu, Q. Zhang, X. Gao, *J. Mater. Chem. A*, **2016**, *4*, 17604–17622.
[6] W. Kranig, C. Boeffel, H. W. Spiess, O. Karthaus, H. Ringsdorf, R. Wüstefeld, *Liq. Cryst.* **1990**, *8*, 375–388.
[7] H. Ringsdorf, R. Wüstefeld, E. Zerta, M. Ebert, J. H. Wendorff, *Angew. Chem. Int. Ed.* **1989**, *28*, 914–918; *Angew. Chem.* **1989**, *101*, 934–938.
[8] D. Markovitsi, H. Bengs, H. Ringsdorf, *J. Chem. Soc. Faraday Trans.* **1992**, *88*, 1275–1279.
[9] S. Zamir, D. Singer, N. Spielberg, E. J. Wachtel, H. Zimmermann, R. Poupko, Z. Luz, *Liq. Cryst.* **1996**, *21*, 39–50.
[10] D. Janietz, R. Festag, C. Schmidt, J. H. Wendorff, *Liq. Cryst.* **1996**, *20*, 459–467.
[11] A. Grafe, D. Janietz, T. Frese, J. H. Wendorff, *Chem. Mater.* **2005**, *17*, 4979–4984.
[12] S. Kumar Varshney, H. Takezoe, D. S. Shankar Rao, *Bull. Chem. Soc. Jpn.* **2008**, *81*, 163–167.
[13] Y. Hanai, M. Jalilur Rahman, J. Yamakawa, M. Takase, T. Nishinaga, M. Hasegawa, K. Kamada, M. Iyoda, *Chem. Asian J.* **2011**, *6*, 2940–2945.
[14] M. Manickam, M. Belloni, S. Kumar, S. K. Varshney, D. S. Shankar Rao, P. R. Ashton, J. A. Preece, N. Spencer, *J. Mater. Chem.* **2001**, *11*, 2790–2800.
[15] J. Li, Z. He, H. Zhao, H. Gopee, X. Kong, M. Xu, X. An, X. Jing, A. N. Cammidge, *Pure Appl. Chem.* **2010**, *82*, 1993–2003.
[16] D. Singer, A. Liebmann, K. Praefcke, J. H. Wendorff, *Liq. Cryst.* **1993**, *14*, 785–794.
[17] Y. Yamamoto, T. Fukushima, A. Saeki, S. Seki, S. Tagawa, N. Ishii, T. Aida, *J. Am. Chem. Soc.* **2007**, *129*, 9276–9277.
[18] T. Hegmann, J. Kain, S. Diele, G. Pelzl, C. Tschierske, *Angew. Chem. Int. Ed.* **2001**, *40*, 887–890; *Angew. Chem.* **2001**, *113*, 911–914.
[19] M. Lehmann, T. Sierra, J. Barberá, J.-L. Serrano, R. Parker, *J. Mater. Chem.* **2002**, *12*, 1342–1350.
[20] K. Kaznacheev, T. Hegmann, *Phys. Chem. Chem. Phys.* **2007**, *9*, 1705–1712.
[21] F. D. Saeva, G. A. Reynolds, L. Kaszczuk, *J. Am. Chem. Soc.* **1982**, *104*, 3524–3525.
[22] P. Davidson, A.-M. Levelut, H. Strzelecka, V. Gionis, *J. Phys. Lett.* **1983**, *44*, 823–828.
[23] H.-P. Werner, W. Grauf, J. U. von Schütz, H. C. Wolf, H. W. Helberg, W. Kremer, A. Aumüller, S. Hünig, *Z. Naturforsch. A* **1989**, *44*, 825–832.
[24] O. Kruglova, E. Mendes, Z. Yildirim, M. Wübbenhorst, F. M. Mulder, J. A. Stride, S. J. Picken, G. J. Kearley, *ChemPhysChem* **2007**, *8*, 1338–1344.
[25] L. A. Haverkate, M. Zbiri, M. R. Johnson, B. Deme, H. J. M. de Groot, F. Lefeber, A. Kotlewski, S. J. Picken, F. M. Mulder, G. J. Kearley, *J. Phys. Chem. B* **2012**, *116*, 13098–13105.
[26] M. Lehmann, M. Hügel, *Angew. Chem. Int. Ed.* **2015**, *54*, 4110–4114; *Angew. Chem.* **2015**, *127*, 4183–4187.
[27] M. Lehmann, M. Dechant, M. Hügel, N. Scheuring, T. Ghosh, *Chem. Eur. J.* **2019**, *58*, 3352–3361.
[28] M. Lehmann, M. Dechant, M. Holzapfel, A. Schmiedel, C. Lambert, *Angew. Chem. Int. Ed.* **2019**, *58*, 3610–3615.
[29] M. Lehmann, P. Maier, M. Grüne, M. Hügel, *Chem. Eur. J.* **2017**, *23*, 1060–1068.
[30] P. Maier, M. Grüne, M. Lehmann, *Chem. Eur. J.* **2017**, *23*, 1018–1021.
[31] M. Lehmann, P. Maier, *Angew. Chem. Int. Ed.* **2015**, *54*, 9710–9714; *Angew. Chem.* **2015**, *127*, 9846–9850.
[32] M. Lehmann, M. Dechant, M. Lambov, T. Gosh, *Acc. Chem. Res.* **2019**, *52*, 1653–1664.
[33] H. M. Harreis, C. N. Likos, M. Ballauff, *J. Chem. Phys.* **2003**, *118*, 1979–1988.
[34] S. Rosenfeldt, E. Karpuk, M. Lehmann, H. Meier, P. Lindner, L. Harnau, M. Ballauff, *ChemPhysChem* **2006**, *7*, 2097–2104.
[35] S. Rosenfeldt, N. Dingenouts, D. Pötschke, M. Ballauff, A. J. Berresheim, K. Müllen, P. Lindner, *Angew. Chem. Int. Ed.* **2004**, *43*, 109–112; *Angew. Chem.* **2004**, *116*, 111–114.
[36] R. K. Harris, R. E. Wasylishen, M. J. Duer, *NMR Crystallography*, John Wiley & Sons **2010**.
[37] Y. Nishiyama, S. P. Brown, Z. Gan, L. Delevoye, L. O'Dell, D. Reichert, M. Vogel, D. Arcon, J. Stebbins, H. Heise, *Modern Methods in Solid-state NMR: A Practitioner's Guide*, Royal Society of Chemistry **2018**.
[38] V. Percec, M. Glodde, T. K. Bera, Y. Miura, I. Shiyanovskaya, K. D. Singer, V. S. K. Balagurusamy, P. A. Heiney, I. Schnell, A. Rapp, H. W. Spiess, S. D. Hudson, H. Duan, *Nature* **2002**, *419*, 384–387.
[39] M. R. Hansen, X. Feng, V. Macho, K. Müllen, H. W. Spiess, G. Floudas, *Phys. Rev. Lett.* **2011**, *107*, 257801.
[40] M. Lehmann, B. Schartel, M. Hennecke, H. Meier, *Tetrahedron* **1999**, *55*, 13377–13394.
[41] T. Wöhrle, J. Kirres, M. Kaller, M. Mansueto, S. Tussetschläger, S. Laschat, *J. Org. Chem.* **2014**, *79*, 10143–10152.
[42] T. Ghosh, L. Gerbig, M. Lambov, M. Dechant, M. Lehmann, *J. Mater. Chem. C* **2020**, *8*, 5562–5571.
[43] N. Hu, R. Shao, Y. Shen, D. Chen, N. A. Clark, D. M. Walba, *Adv. Mater.* **2014**, *26*, 2066–2071.
[44] H. Meier, M. Lehmann, U. Kolb, *Chem. Eur. J.* **2000**, *6*, 2462–2469.
[45] B. Donnio, B. Heinrich, H. Allouchi, J. Kain, S. Diele, D. Guillon, D. W. Bruce, *J. Am. Chem. Soc.* **2004**, *126*, 15258–15268.
[46] L. K. Minacheva, V. S. Sergienko, S. B. Strashnova, O. V. Avramenko, O. V. Koval'chukova, O. A. Egorova, B. E. Zaitsev, *Crystallogr. Rep.* **2005**, *50*, 72–77.
[47] J. N. Brown, L. D. Cheung, L. M. Trefonas, R. J. Majeste, *J. Cryst. Mol. Struct.* **1974**, *4*, 361–371.
[48] M. Lehmann, C. Köhn, H. Meier, S. Renker, A. Oehlhof, *J. Mater. Chem.* **2006**, *16*, 441–451.
[49] M. Lehmann, M. Jahr, B. Donnio, R. Graf, S. Gemming, I. Popov, *Chem. Eur. J.* **2008**, *14*, 3562–3576.
[50] C. Tschierske , *Microsegregation in Liquid Crystalline Systems: Basic Concepts. In Handbook of Liquid Crystals, Vol. 5: Non-Conventional Liquid Crystals*, 2nd ed. (Eds. J. W. Goodby, P. J. Collings, T. Kato, C. Tschierske, H. F. Gleeson, P. Raynes), Wiley-VCH: Weinheim, Germany **2014**, Chapter 1.
[51] O. S. Makin, P. Sikorski, L. C. Serpell, *J. Appl. Crystallogr.* **2007**, *40*, 966–972.
[52] A. Natansohn, *Polym. Bull.* **1989**, *21*, 217–220.
[53] A. Natansohn, *Macromolecules* **1991**, *24*, 1662–1669.
[54] P. A. Heiney, http://www.datasqueezesoftware.com/.
[55] P. Scherrer, *Nachr. Ges. Wiss. Goettingen Math.-Phys. Kl.* **1918**, *2*, 98–100.

Manuscript received: April 28, 2020
Revised manuscript received: June 24, 2020
Accepted manuscript online: June 25, 2020